Response of seismicity to Coulomb stress triggers and shadows of the 1999 M_w = 7.6 Chi-Chi, Taiwan, earthquake

Kuo-Fong Ma and Chung-Han Chan
Institute of Geophysics, National Central University, Chung-Li, Taiwan

Ross S. Stein
U.S. Geological Survey, Menlo Park, California, USA

Received 16 August 2004; revised 23 March 2005; accepted 4 April 2005; published 28 May 2005.

[1] The correlation between static Coulomb stress increases and aftershocks has thus far provided the strongest evidence that stress changes promote seismicity, a correlation that the Chi-Chi earthquake well exhibits. Several studies have deepened the argument by resolving stress changes on aftershock focal mechanisms, which removes the assumption that the aftershocks are optimally oriented for failure. Here one compares the percentage of planes on which failure is promoted after the main shock relative to the percentage beforehand. For Chi-Chi we find a 28% increase for thrust and an 18% increase for strike-slip mechanisms, commensurate with increases reported for other large main shocks. However, perhaps the chief criticism of static stress triggering is the difficulty in observing predicted seismicity rate decreases in the stress shadows, or sites of Coulomb stress decrease. Detection of sustained drops in seismicity rate demands a long catalog with a low magnitude of completeness and a high seismicity rate, conditions that are met at Chi-Chi. We find four lobes with statistically significant seismicity rate declines of 40–90% for 50 months, and they coincide with the stress shadows calculated for strike-slip faults, the dominant faulting mechanism. The rate drops are evident in uniform cell calculations, 100-month time series, and by visual inspection of the $M \geq 3$ seismicity. An additional reason why detection of such declines has proven so rare emerges from this study: there is a widespread increase in seismicity rate during the first 3 months after Chi-Chi, and perhaps many other main shocks, that might be associated with a different mechanism.

Citation: Ma, K.-F., C.-H. Chan, and R. S. Stein (2005), Response of seismicity to Coulomb stress triggers and shadows of the 1999 M_w = 7.6 Chi-Chi, Taiwan, earthquake, *J. Geophys. Res.*, *110*, B05S19, doi:10.1029/2004JB003389.

1. Introduction

[2] Advocates of static stress transfer argue that aftershocks and subsequent main shocks often occur in regions that experienced an increase in Coulomb stress caused by the main shock, and that earthquakes become less prevalent than before the main shock in regions subject to a Coulomb stress drop (see reviews by *Harris* [1998], *Stein* [1999], and *King and Cocco* [2001]). Most work on this hypothesis has concentrated on strike-slip main shocks, whose stress change does not vary greatly with depth. For thrust faulting, the stress change is depth-dependent [*Lin and Stein*, 2004], and thus the downdip geometry and slip of the source fault, and the depth of aftershocks become essential to Coulomb analysis. The 20 September 1999 M_w = 7.6 Chi-Chi, Taiwan, earthquake on the Chelungpu fault is probably the world's best recorded continental thrust event, with well determined spatial slip models from seismic, strong motion, and geodetic data. Equally important for this study, background seismicity and aftershock sequence are also recorded in unprecedented detail (Figure 1), making it ideal for investigation.

[3] Several studies [e.g., *Ma et al.*, 2001; *Zeng and Chen*, 2001; *Chi et al.*, 2001; *Ji et al.*, 2003] have illuminated the kinematics of the Chi-Chi rupture process. Results of these studies show consistent features, with high slip in the northern portion of the fault. Aftershocks, recorded by the Central Weather Bureau Seismographic Network (CWBSN), are widely distributed over central Taiwan. During the first month after the main shock, nine $M > 6.0$ aftershocks occurred near the source region of the main shock, yielding more disastrous damage, and providing a further data set for stress transfer analysis.

[4] Using the detailed spatial slip distribution of the Chi-Chi earthquake source, we calculated the Coulomb stress changes following *Toda et al.* [1998], which we compare to the seismicity rate changes derived from the 100-month seismic record centered on the main shock. We place particular emphasis on the response of seismicity to the broad lobes of calculated stress increase (the trigger zones), and stress decrease (the stress shadows), and on whether the

0148-0227/05/2004JB003389$09.00

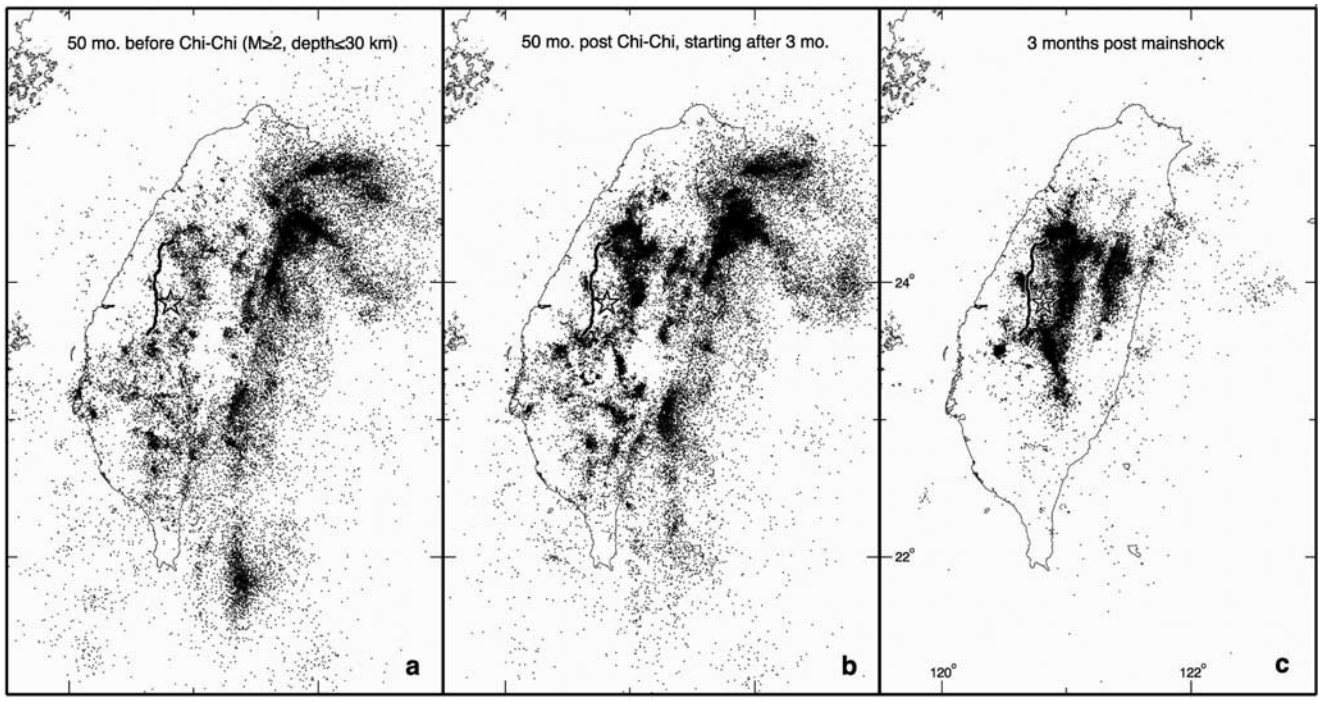

Figure 1. $M \geq 2$ seismicity during (a) the 50 months preceding the 1999 Chi-Chi earthquake, (b) 3–53 months after the main shock, and (c) the first 3 months after the main shock. The seismic station distribution is shown in Figure 3.

stress imparted to the aftershock rupture planes promoted their failure.

[5] Several Coulomb stress analyses of the 1999 Chi-Chi earthquake have already been carried out with the first year of aftershocks, independent of their focal mechanisms. *Wang and Chen* [2001] examined stress transferred to the aftershock triggering and the surrounding faults, employing a Chi-Chi source model derived from GPS data by *Wang et al.* [2001]. Unfortunately, this source model is largely inconsistent with those derived from strong motion, teleseismic and GPS data. *Wang et al.* [2003] calculated the static stress transfer from "stress grams" derived directly from seismograms rather than from elastic calculation. The stress patterns they found are inconsistent with the expected stress change pattern associated with a thrust fault [*Lin and Stein*, 2004], and with the observed aftershock distribution, and are thus difficult to evaluate or verify.

2. Changes in Seismicity Associated With the Chi-Chi Earthquake

2.1. Seismicity

[6] Our goal is to measure long-term seismicity rate changes caused by the 1999 Chi-Chi earthquake. Here, seismicity rate change is simply the rate of earthquakes after the main shock, divided by the rate beforehand. To permit visual inspection of the numerical results, we consider equal 50-month periods before and after the earthquake. We choose this duration because network detection improved substantially in 1994, when the Taiwan Telemetered Seismographic Network was upgraded and transferred to the Central Weather Bureau to become the Taiwan Seismographic Network, or CWBSN. The seismicity rate is reckoned independent of magnitude, and so it is essential that we count earthquakes above the minimum magnitude of completeness, M_c [*Wiemer and Wyss*, 2000].

[7] For the post-Chi-Chi period, we consider the 50-month period beginning 3 months after the main shock, after which the seismicity rate declines become clear. As will be evident from the time series we will introduce, there is a widespread increase in seismicity throughout Taiwan during the first 1–3 months after the Chi-Chi main shock. During the first 1–3 months after the main shock, M_c is also unusually high, presumably because the order-of-magnitude increase in seismicity overwhelms routine processing. After this period, several areas exhibit seismicity rate declines that we will explore. We will show both the 3-month and 50-month post-Chi-Chi periods in our figures and time series.

[8] The distribution of $M \geq 2.0$ seismicity before and after the occurrence of the 1999 $M = 7.6$ Chi-Chi earthquake (compare Figures 1a and 1b) is surprisingly similar (as we will show, the catalog is complete to $M = 2$ within the island of Taiwan). The earthquakes are a consequence of the collision of the Philippine Sea Plate and Eurasian Plate along the Rukyu Arc, and the opening of Okinawa trough in northeastern Taiwan. Although the rate of seismicity within several fault lengths of the Chi-Chi epicenter is more than hundred times higher after the main shock than before, the spatial distribution in Figure 1b is only subtly changed from the pre-Chi-Chi period in Figure 1a. In fact, if one were to examine Figures 1a and 1b separately, it would be difficult to tell which map contains the Chi-Chi aftershocks. We suggest that the similarity arises because stress increases amplify the rate of background seismicity, while stress

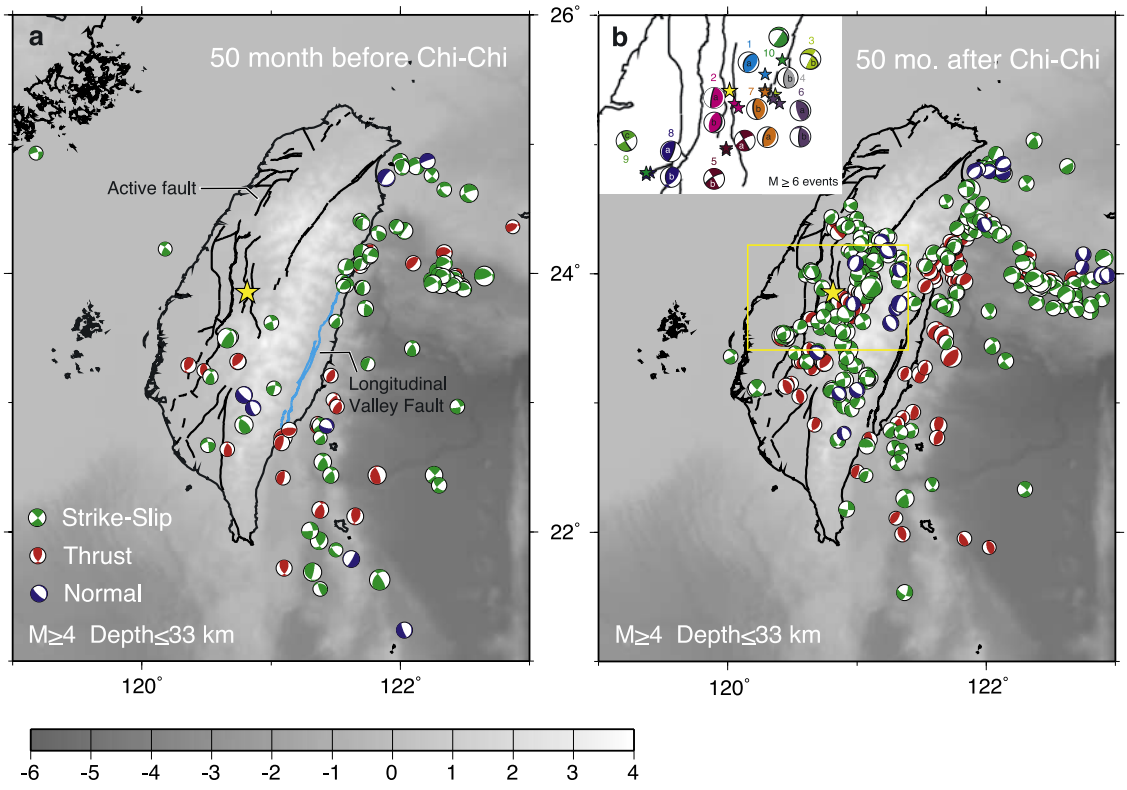

Figure 2. Focal mechanism distribution for events in and around Taiwan (a) before and (b) after the Chi-Chi main shock. The focal mechanisms are the available moment tensor solutions from Broadband Array in Taiwan for Seismology (BATS). M_w is about 0.19 less than the local magnitude (M_L) determined in the catalog, and M_c = 4.2. The $M \geq 6$ shocks are shown in the Figure 2b inset, with the preferred rupture plane indicated by the bold line. Event numbers correspond to Table 3; references are a, *Chi and Dreger* [2004]; b, *Yen* [2002]; and c, *Ma and Wu* [2001].

decreases suppress the background seismicity. This prediction of rate/state friction [*Dieterich*, 1994] regards aftershocks simply as dramatically higher rates of background seismicity, as investigated by *Toda and Stein* [2003] for the 1997 Kagoshima, Japan, earthquakes and by *Toda et al.* [2005] for the 1992 Landers/1999 Hector Mine sequence.

2.2. Focal Mechanisms

[9] Figure 2 shows the distribution of the focal mechanisms before and after the Chi-Chi earthquake. The focal mechanisms are mainly strike slip and thrust. There is an extended zone of seismicity in the fold and thrust belt near the ends of the Chelungpu fault dominated by strike-slip mechanisms that cannot be associated with mapped active faults (Figure 2b). The focal mechanism distribution is generally similar before and after the Chi-Chi earthquake, except for a relative increase in strike-slip mechanisms to the southeast of the Chelungpu fault and well offshore to the east. In addition, thrust events may be relatively more common on the central east coast after the Chi-Chi earthquake.

[10] For this new compilation, we used moment tensors inverted from waveforms of the Broadband Array in Taiwan for Seismology (BATS) [*Kao et al.*, 2002; *Liang et al.*, 2003, 2004a]. Since 2001, the Data Management Center of the Institute of Earth Sciences (DMC-IES) has reported and archived moment tensor solutions obtained by inverting BATS waveforms of felt earthquakes that occurred since July 1995 [*Liang et al.*, 2004b]. The DMC-IES has reported a completed moment magnitude (M_w) of 4.2 before 2001, and 3.9 since that time. The compilation includes 101 $M_w \geq$ 4.0 focal mechanisms before the Chi-Chi main shock, and 354 afterward (depths < 33 km), and can be accessed from http://eqkc.earth.ncu.edu.tw/FocalMech.

2.3. Seismicity Rate Changes

[11] To examine the seismicity rate change, we first calculate the minimum magnitude of completeness, M_c, for the pre- and post-Chi-Chi periods (Figure 3), using ZMAP [*Wiemer*, 2001]. Where seismicity rates are low, we resort to a larger cell size to capture a sufficient number of earthquakes. M_c is generally stable throughout this 100-month period, except in the north central part of Taiwan (24° latitude), where M_c is higher after Chi-Chi. For the interior of Taiwan, $M_c \leq 2$; for regions within about 100 km of the coastline, $M_c \leq 3$.

[12] The seismicity rate change is calculated in Figure 4. Within Taiwan, $M \geq 2$ is used with a 10 × 10 km cell size; for most offshore areas, $M \geq 3$ is used with a 20 × 20 km cell size. During the first 3 months, most of Taiwan experiences a seismicity rate increase, and these increases are uncorrelated with the distribution of $M \geq 6$ aftershocks

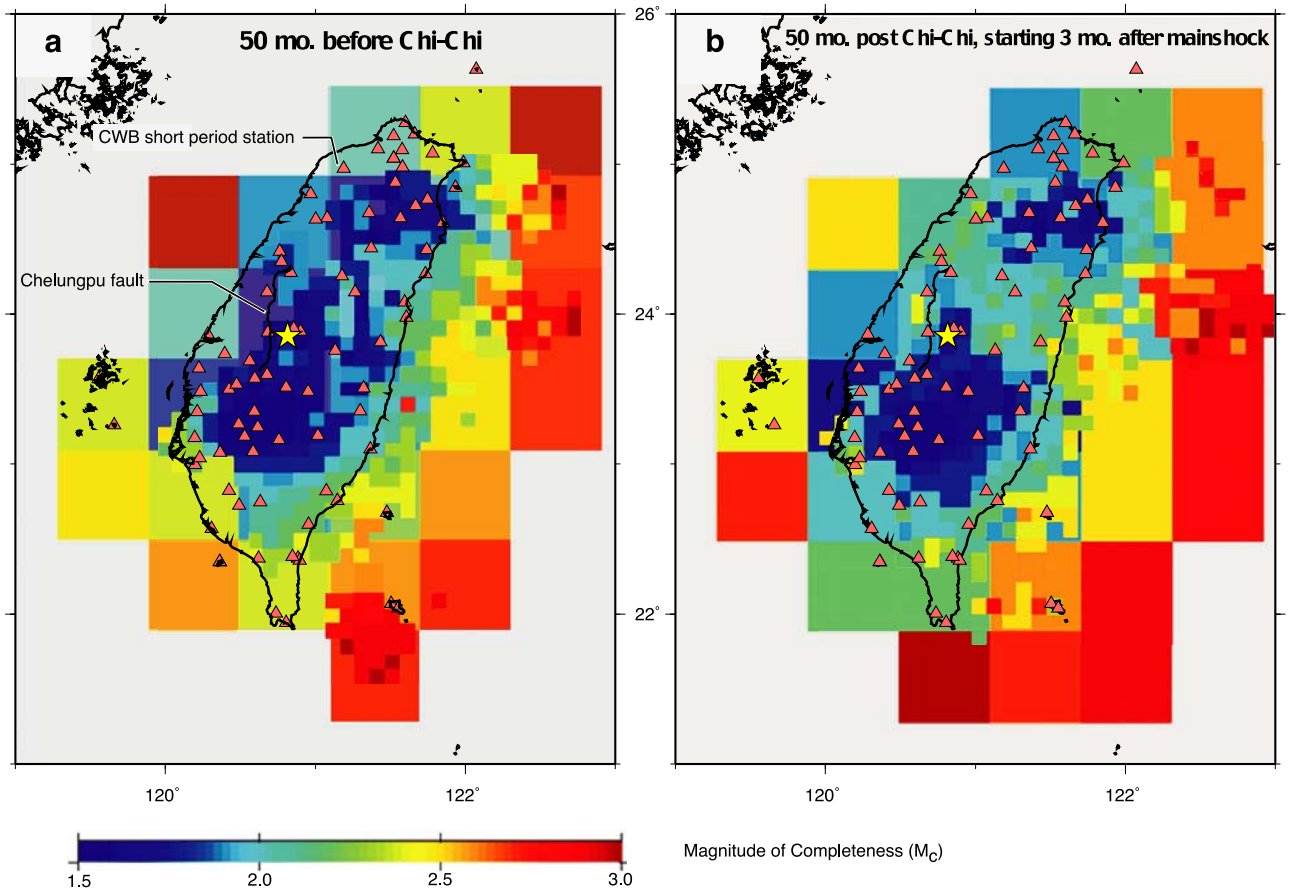

Figure 3. Minimum magnitude of completeness, M_c, for 50-month (a) pre- and (b) post-Chi-Chi periods, calculated from ZMAP. The post-Chi-Chi period begins 3 months after the main shock are omitted. The cell size is increased offshore to capture sufficient earthquakes for M_c determination.

(Figure 4a). During the subsequent 50 months, a broad area of seismicity rate increase is seen over much of central Taiwan, but there are weaker and more restricted zones of seismicity rate drop in some surrounding areas (Figure 4b). Beginning about 25 months after the Chi-Chi shock, the seismicity rate decreases in two of the regions become stronger and enlarge (Figure 4c). As a control test on these calculations, we divided the 50 pre-Chi-Chi months into two equal periods and calculated the seismicity rate change for the second period relative to the first. The resulting map has an equal distribution of white, red, and blue cells, with no regions of uniform color more than a few cells in size. There is also no evidence from this test of precursory seismicity or quiescence in the future epicentral area.

[13] Although Figure 4 is an objective measure of the seismicity rate change, where there is a high density of $M \geq 2$ shocks it is nevertheless difficult to see the rate changes by comparing Figures 1a and 1b. So, in Figure 5, the $M \geq 3$ seismicity is shown. Because the pre-Chi-Chi shocks are red and the post-Chi-Chi shocks are blue, by visual inspection areas dominated by red correspond to seismicity rate drops. The sites of rate increase, highlighted in light orange, dominate central Taiwan. The seismicity rate decreases are highlighted in turquoise and given a locality name. Although these regions are evident in Figure 4, in our judgment their full extent is more apparent in Figure 5. While we do not use the zones shown in Figure 4 for statistical analysis, it is important that the rate declines are readily visible.

[14] Time series of seismicity in each of the five regions, plotted at the highest M_c of the pre- or post-Chi-Chi periods for each zone to ensure completeness, are shown in Figure 6. We have carried out no declustering; all recorded earthquakes appear in the time series in Figure 6 and in the maps. All of the time series in Figure 6 exhibit a spike in seismicity during the first few months after Chi-Chi, with the top four series followed by a decline of 38–90%. The mean pre- and post-Chi-Chi rates are shown in the plots, with the period 3–53 months after Chi-Chi used. To assess whether the premean and postmean differ, we computed the Student's t distribution probability function, $A(t|\nu)$, where t is calculated the condition in which the variances of the pre- and post-Chi-Chi variances are be the same, and ν is the degrees of freedom [*Press et al.*, 1992, equations 6.4.7–6.4.9 and 12.2.3–12.2.4]. In all cases the rate changes are significant at the 99.9% level (Table 1).

[15] *Marsan* [2003] and *Felzer and Brodsky* [2005] argue that seismicity rate declines are absent in the vicinity of the main shocks they have examined. Thus we accord particular attention to the identification of seismicity rate decreases. An apparent rate decrease can result from a decaying sequence of aftershocks associated with a main shock that

struck during the pre-Chi-Chi period, rather than with a change in rate associated with the Chi-Chi shock. So, we studied time series of all rate decrease (blue) cells in Figure 4b, and excluded from consideration any cell influenced by such an aftershock sequence. The seismicity identified in Figures 5 and 6 is free from such effects.

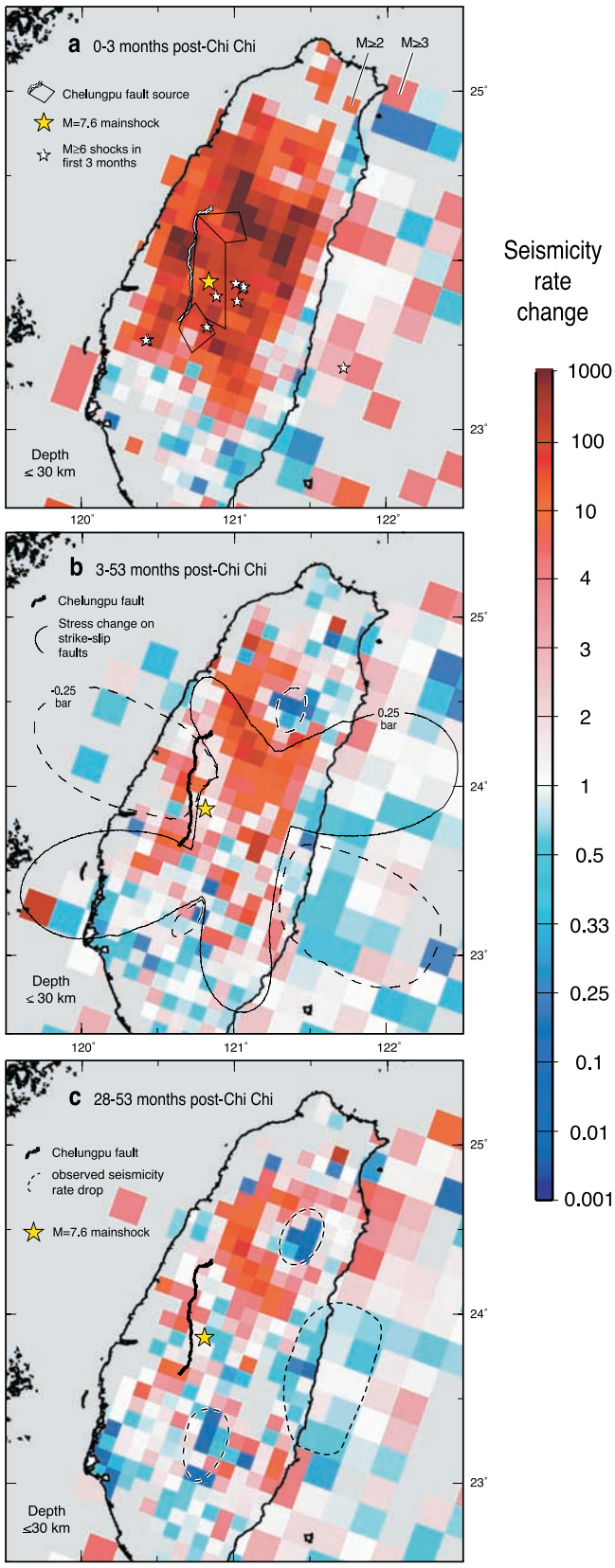

3. Coulomb Stress Changes Caused by the Chi-Chi Earthquake

3.1. Resolving Stress Changes on Receiver Faults

[16] The static Coulomb stress change $\Delta CFF = \Delta\tau + \mu'\Delta\sigma$, where $\Delta\tau$ is the shear stress change (reckoned positive in the fault slip direction), μ' is effective friction coefficient (after accounting for pore fluid pressure), and $\Delta\sigma$ is the normal stress change (positive when unclamped) [*King et al.*, 1994; *Toda et al.*, 1998]. Fault friction μ' is often inferred to be 0.4–0.8 for faults with relatively little cumulative slip, which tend to be rough, and 0.0–0.4 for faults with great cumulative slip or high pore pressure, which tend to be smooth or well lubricated [*Parsons et al.*, 1999]. Here, we use $\mu' = 0.4$, because we are unable to assign a value with confidence and thus choose a value midway between the possible extremes. We experimented with $0.0 \leq \mu' \leq 0.8$; results are modestly sensitive to μ'. Major faults, such as the Chelungpu (which has slipped at 8.5 mm/year for the past 1900 years [*Chen et al.*, 2004; *Ma and Chiao*, 2003]) may possess low friction, but for most faults the data is insufficient.

[17] The Coulomb stress change is a tensor quantity, and so depends not only on the source fault geometry and slip, but also on the geometry and rake of the "receiver" or target faults that surround the source. There are two principal approaches to calculating the Coulomb stress changes on receiver faults. One can resolve the Coulomb stress changes on faults with known geometry and rake, or one can resolve stress changes on "optimal planes" constrained by the tectonic or regional stress. In this study we pursue both.

[18] We resolve the Coulomb stress change on planes optimally oriented for failure with respect to the combined regional stress and earthquake stress change in an elastic half-space [*King et al.*, 1994]. At the magnitude of completeness, M_c, of 2.0–3.0, faults on which earthquakes can occur are quite small, with rupture lengths as little as 50 m. At this scale, there are likely myriad faults with different geometries and rakes at any given position in the crust. The optimum planes are those that receive the most positive Coulomb stress change at every point. The regional stress is typically inferred from focal mechanisms far from the source fault, borehole stress inversions, or the geodetically determined strain rate tensor. At every calculation point, the earthquake stress is added to the regional stress to get a new, local stress tensor. The optimum planes are oriented at an

Figure 4. Calculated seismicity rate change associated with the Chi-Chi earthquake. Postseismic periods are compared to the 50 months before the Chi-Chi earthquake. For the $10 \times 10 \times 30$ km cells within Taiwan, $M \geq 2$ shocks are used; for the $20 \times 20 \times 30$ km cells, $M \geq 3$ are used, on the basis of the distribution of M_c shown in Figure 3. (a) The first 3 months post-Chi Chi. (b) The 50 months post-Chi Chi, starting 3 months after the main shock, with modeled stress-change contours from Figure 7c. (c) The 25 month-period starting 28 months after Chi-Chi.

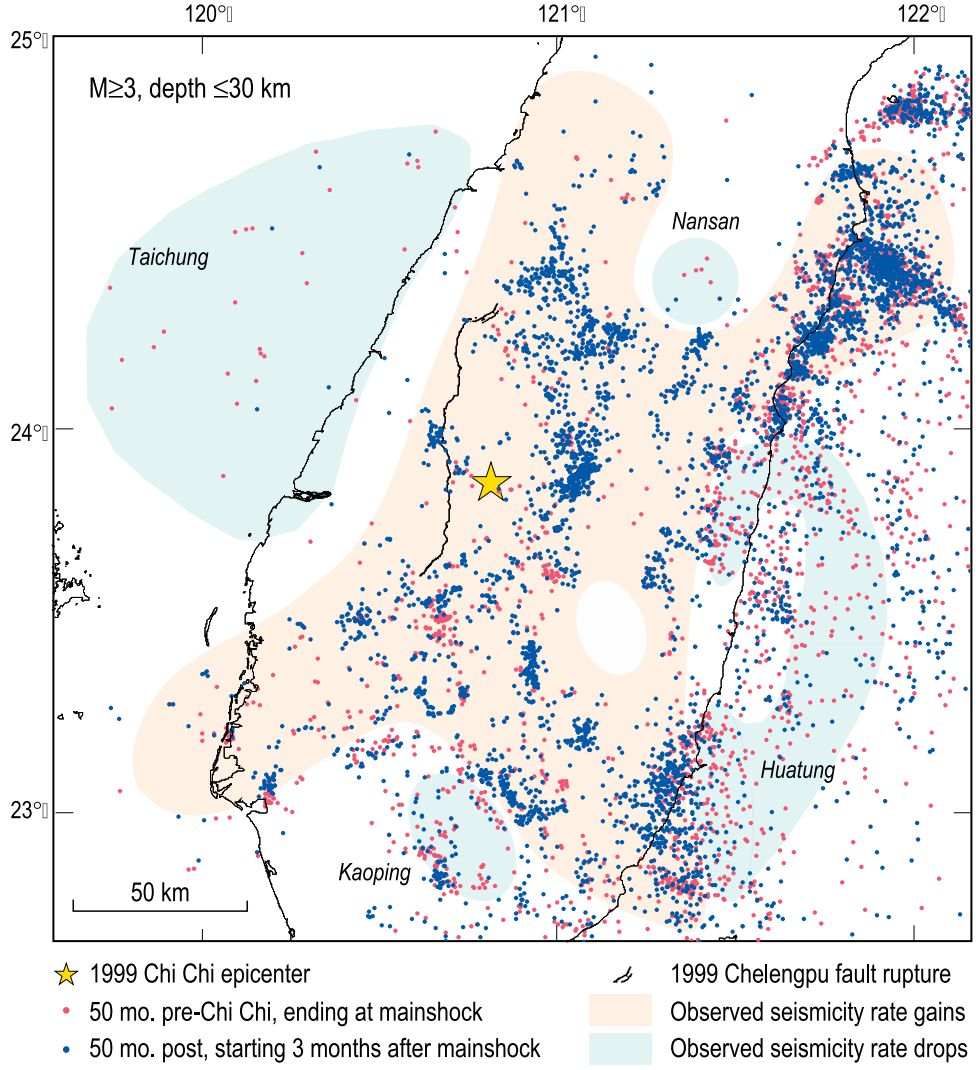

Figure 5. $M \geq 3$ seismicity during the 50 months before and after the Chi-Chi earthquake. On the basis of the $M \geq 3$ observations and the fixed cell size calculations of Figure 4, sites of apparent seismicity rate increase are light orange; sites of decrease are turquoise. Site names correspond to Figure 6.

angle to this local tensor determined by the friction coefficient, μ'.

[19] The relationship between the principal compression axis and the optimal planes is shown in Figures 7a and 7b at the top of each map. The optimal strike-slip planes dip vertically; the optimal thrust plans dip at shallow angle and strike perpendicular to the axis of principal compression. The internal angle between the optimal planes is a function of friction, μ'. For $\mu' = 0$, the two optimal planes are mutually orthogonal; for a high value of friction, they form at acute angles to each other. For central Taiwan, a regional compressive stress of 100 bars acting in the direction of the stress axis of the Philippine to the Eurasian plates [*Seno*, 1977] is used, with a 30-bar compression oriented vertically; the full stress tensor is listed in Table 2.

3.2. Coulomb Stress Change for an Idealized Chi-Chi Source

[20] The Coulomb stress imparted by the Chi-Chi earthquake is perhaps best understood by considering Figure 7, the maximum Coulomb stress change over a depth of 5–30 km for a simplified Chi-Chi source with $M_w = 7.6$. Here, we make an additional assumption that at every point on the Earth's surface, aftershocks (or strictly, seismicity rate increases) will occur at the depth where the Coulomb stress change is most positive, an approach introduced by *King et al.* [1994] and investigated by *Lin and Stein* [2004] for thrust fault seismicity. Unlike the Coulomb stress calculated at a particular depth horizon, the maximum Coulomb stress change, when integrated around a source, will be positive; the trigger zones will enlarge and the stress shadows will shrink. This approach is most amenable to examinations of seismicity rate changes or aftershocks over the entire brittle crust, or the uppermost 25–30 km. In Figures 7a and 7b, the source is pure thrust slip; the observed left-lateral component is ignored. Figure 7a shows the stress changes on surrounding thrust faults; Figure 7b shows the stress changes on strike-slip faults. Stress changes on strike-slip receiver faults extend farther from the source than for thrust faults,

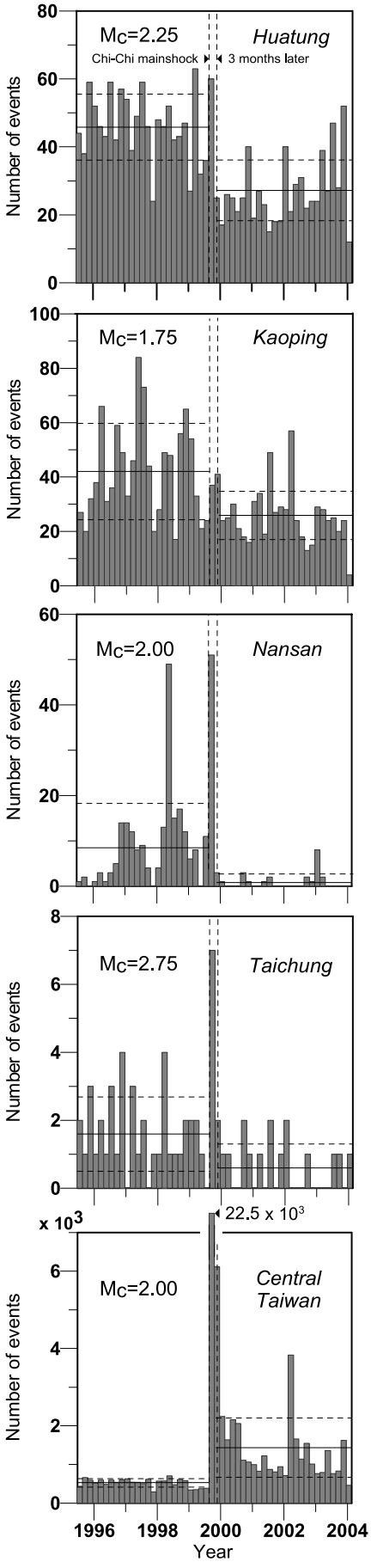

the trigger zones forming a characteristic "butterfly" pattern [*Stein et al.*, 1994], and the shadows are stronger.

[21] A calculation that more closely resembles the Chi-Chi earthquake is shown in Figures 7c and 7d, for a source with a strike of 3° and a rake of 66° (the centroid moment tensor (CMT) rake for the Chi-Chi main shock), and with the regional compression axis is oriented NW-SE, as in central Taiwan. For thrust faults, there is a broad zone of stress increase in central Taiwan; for strike-slip faults, the butterfly wings become asymmetric, but the four stress shadows, large shadows extending offshore and small ones to the north and south of Taiwan, persist.

[22] Although we will next introduce a detailed model of the Chi-Chi source, even this simple model captures much of the observed pattern of seismicity rate change evident in Figures 4b and 5. It is also evident that the observed pattern of seismicity rate changes most resembles the expectation for strike-slip than thrust faults, and so we superimpose the stress contours of Figure 7d on Figure 4b. Although thrust faults lace central Taiwan, the majority of the aftershock focal mechanisms, particularly in central Taiwan, are strike slip (Figure 2).

3.3. Coulomb Stress Change for a Detailed Chi-Chi Source

[23] For a rigorous comparison between stress change and seismicity change, we use the full variable-slip source of *Ji et al.* [2003], inverted from GPS displacements, strong motion data, and teleseismic waveforms. The coseismic source is defined by 324 slip patches with variable rake and slip on three rectangular planar surfaces, each dipping 29° (Figure 8). The resulting Coulomb stress changes on optimally oriented strike-slip, thrust, and normal faults are shown in Figure 9. Because of the complex fault geometry and slip heterogeneity, the stress change varies with depth and along with strike. Close to the Chelungpu fault source, the stress generally increases because of the slip variability, which causes spikes in stress.

3.4. Stress Change Analyzed by Depth and Focal Mechanism

[24] The stress patterns for thrust (Figure 9a) and strike-slip (Figure 9b) receiver faults are similar to that shown in Figures 7c and 7d for an idealized Chi-Chi source, and the pattern for normal receiver faults (Figure 9c) is roughly opposite as that for thrusts. In comparison to the maximum Coulomb stress change over a great depth range (Figure 7), the stress shadows are larger in Figure 9. This is because the extent of the triggering zones and shadows will be approximately equal in each depth slice, and so ~50% of a random earthquake sample would lie in regions of positive Coulomb stress change.

Figure 6. Time series of the zones of seismicity rate drop identified in Figure 5, each at $M \geq M_c$ so that detection is uniform throughout the period shown. For each zone, M_c was determined independently in ZMAP [*Wiemer*, 2001]. The horizontal lines mark the mean and standard deviation of the pre and post-Chi-Chi seismicity rates, with the 3-month period after Chi-Chi excluded. The significance of the rate changes is listed in Table 1; all reach the 99.9% level.

Table 1. Significance of the Mean Seismicity Rate Changes Before and After the Chi-Chi Main Shock Shown in Figure 6[a]

Location	Seismicity Rate Change	Student's t Statistic	Degrees of Freedom ν	Significance of Change A, %
Huatung	0.59	6.97	47.5	100.00
Kaoping	0.62	4.01	35.0	99.97
Nansan	0.10	3.74	25.7	99.91
Taichung	0.38	3.78	40.6	99.95
Central Taiwan	2.74	5.88	25.0	100.00

[a]All changes exceed the 99.9% level; t is the Student's t distribution, ν is the number of degrees of freedom given the observed variance before and after the main shock, and A is the probability that the two means are different.

[25] To examine the correlation of the Coulomb stress changes to earthquakes with focal mechanisms, in Figure 9, earthquakes before (green) and after Chi-Chi (magenta) are also plotted in the depth slices by rake angle (thrust, 45° to 135°; strike slip, −45° to 45°; normal, −45° to −135°). Only the post-Chi-Chi mechanisms should exhibit a correlation with the Coulomb stress change. The pre-Chi-Chi ratio is 45%, roughly what would be expected for an uncorrelated distribution. In contrast, some 75% of the post-Chi-Chi focal mechanisms occur in zones of Coulomb stress increase. This percentage is the same for all three mechanisms, despite the much higher percentage of strike-slip mechanisms, which comprise 64% of the focal mechanism catalog.

3.5. Stress Resolved on All $M \geq 4$ Earthquakes With Focal Mechanisms

[26] While Figure 9 affords visual inspection of the relationship between the calculated stress and the focal mechanisms, and shows the depth distribution of stress and earthquakes, we can more fully exploit the focal mechanisms by calculating the Coulomb stress change on the nodal planes of each of the 354 events. Unlike Figure 9, which simply classifies events into one of three mechanisms and four depth ranges, here we resolve the stress change at the observed depth and for the observed strike, dip, and rake. For zero friction (μ'), the Coulomb stress change on both nodal planes is the same, but for nonzero friction it is different, introducing a nodal plane ambiguity. In Figure 10a, we bin the mechanisms by the resolved Coulomb stress change as a function of focal mechanism, under the zero friction assumption. For 74% of the thrust, 61% of the strike slip, and 63% of the normal events, the calculated stress change exceeds 0.01 bar, whereas for random occurrence, failure would be promoted on about 50% of the events. For stress changes > |0.1 bar|, the comparison is stronger still: 85% of the thrust, 65% of the strike slip, and 80% of the normal events are brought close to Coulomb failure. These percentages rise slightly for strike-slip and thrust mechanisms if we omit the first 3 months of focal mechanisms.

[27] To include the role of unclamping in promoting failure, which is likely important [*Hardebeck et al.*, 1998; *Parsons et al.*, 1999; *Seeber and Armbruster*, 2000; *Lin and Stein*, 2004], we must contend with the nodal plane ambiguity. We do so for $\mu' = 0.4$ by comparing post- to pre-Chi-Chi mechanisms shown in Figure 2a. If both nodal planes are brought closer to failure, we report the smaller stress change of the two; if failure is promoted on only one plane, we report its value. If both planes receive a Coulomb stress drop, we report the smaller decrease. Following *Hardebeck et al.* [1988], the selection criterion is applied to both pre- and post-Chi-Chi events in Figures 10b and 10c, so any biases in the selection criteria are normalized, as only the differences in the percentages are used. As shown in Figure 10d, the percentage of thrust events with Coulomb stress changes > |0.1 bar| rose by 26% after Chi-Chi (from 37 to 63%); for strike-slip events, it rose by 18% (from 32 to 50%). The pre-Chi-Chi sample of five normal events is too small to be reliable.

3.6. Stress Imparted to $M \geq 6$ Aftershocks

[28] Thus far, we have focused on the 92,000 $M \geq 2$ earthquakes, and the smaller but richer sample of $M \geq 4$ focal mechanisms. For earthquake hazards, however, we are most concerned about $M \geq 6$ shocks, of which 10 struck Taiwan during the first year after the main shock (Figure 2b inset and Figure 4a). The quality of the Taiwan network makes it possible to attempt to distinguish the likely fault plane from the auxiliary plane, which is needed for the stress analysis with nonzero μ'. *Yen* [2002] used strong motion waveforms to determine the likely rupture planes and spatial slip distributions, and relocated the aftershocks using HypoDD [*Waldhauser and Ellsworth*, 2000]. *Chi and Dreger* [2004] inverted strong motion data for the finite fault source parameters, and derived a preferred plane from forward testing of focal mechanisms, hypocenters and rupture velocities (Table 3). Most of the likely fault planes dip to the east (Figure 2b inset and Table 3), consistent with the fold and thrust tectonics.

[29] For the 10 shocks, there are 16 preferred rupture planes based on analyses by *Ma and Wu* [2001], *Yen* [2002], and *Chi and Dreger* [2004]. Failure on 12–14 of the preferred rupture planes, or 7–9 of the earthquakes, is calculated to have been promoted by the Chi-Chi main shock alone, and by the cumulative stress change from Chi-Chi and the successive $M \geq 6$ shocks; the median stress change on the 16 planes is +4.4 bars (Table 3). For $\mu' = 0.0$, the median stress change is +3.53 bars. Thus even if the fault plane assignments are incorrect, the shear stress was substantially increased on the aftershock rupture planes.

4. Discussion and Conclusions

[30] This study benefited from an extraordinary catalog of $M \geq 2$ earthquakes with nearly uniform dense station coverage for 50 months before and 50 months after the Chi-Chi earthquake (Figures 1 and 3), without which measurement of seismicity rate drops associated with large earthquakes is not possible. We also were able to subject 455 $M \geq 4$ relocated earthquakes with focal mechanisms to stress analysis, aided by a 325-patch earthquake source model. Finally, we could examine the stress imparted to 10 $M \geq 6$ aftershocks for which the likely rupture planes have been distinguished (Figure 2b inset). From this work we draw several principal conclusions:

4.1. Aftershocks and the Permanence of Background Seismicity Patterns

[31] The pre- and post-Chi-Chi patterns of seismicity patterns are surprisingly similar, particularly given that the

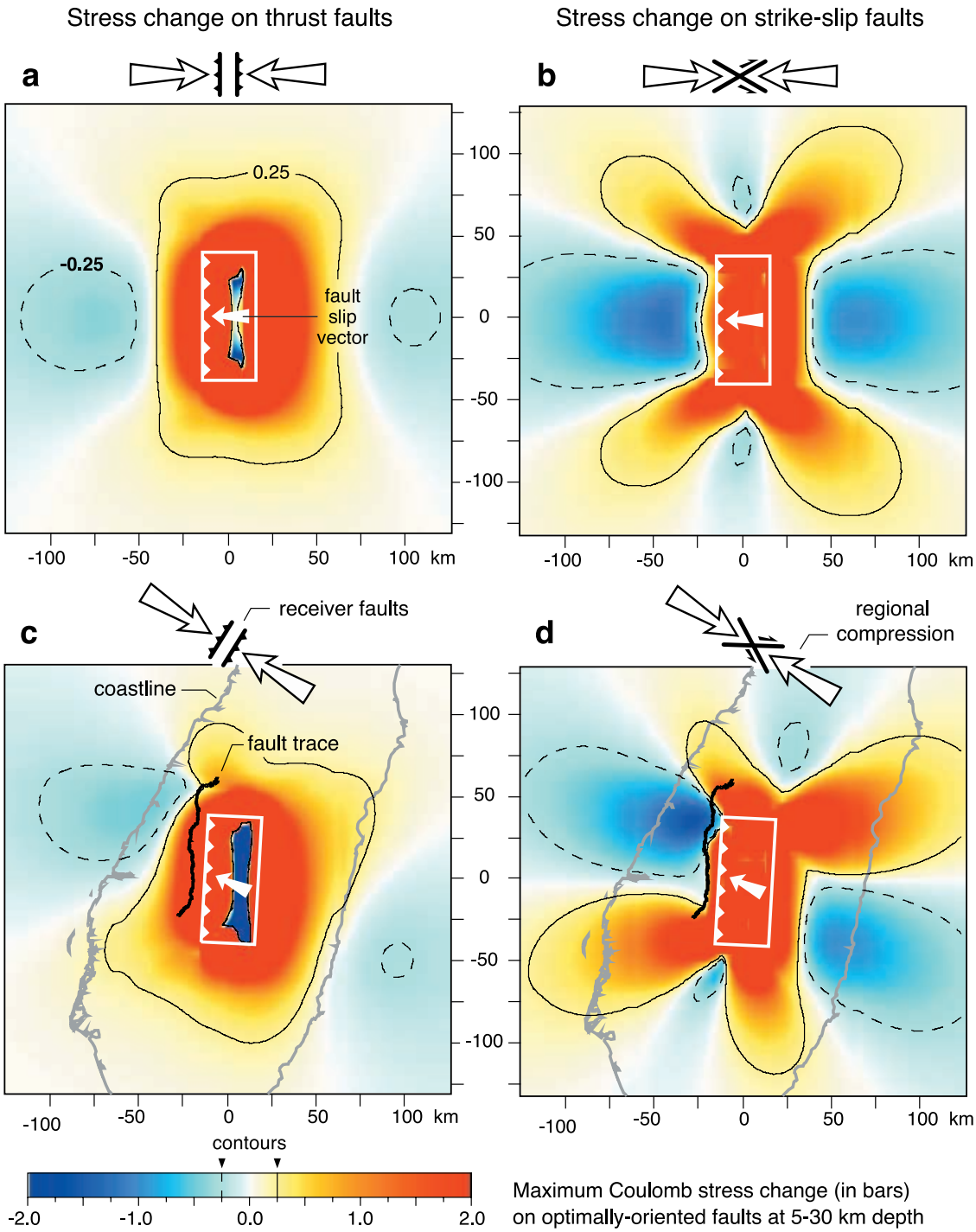

Figure 7. Maximum Coulomb failure stress change within the seismogenic crust for idealized Chi-Chi ruptures, for $\mu' = 0.4$. The source is 78 km long and dips 29°E. (a, b) Stress resolved on optimally oriented thrust or strike-slip faults with E-W regional compression and a source rake of 90°. (b, c) Stress resolved on optimally oriented thrust and strike-slip faults with 122° regional compression and a source strike of 3° and rake of 66°.

postseismic period contains almost 14,000 more shocks than the preceding period of the same duration (Figures 1a and 1b). This, in our judgment, is an indication that seismicity is not turned on or off by a main shock, but rather, the rate of earthquakes rises in areas of Coulomb stress increase, and falls in regions of stress decrease, as predicted by rate/state friction [*Dieterich*, 1994; *Toda et al.*, 2005]. Because of this, the pattern of seismicity remains largely unchanged, with earthquakes simply becoming denser in areas of stress increase and sparser in areas of stress decrease. Further, sites of high background seismicity are very sensitive to small stress increases or decreases, and

Table 2. Regional or Tectonic Stress Tensor Used to Calculate the Coulomb Stress Change on Optimally Oriented Faults in Figures 7b, 7c, and 9[a]

	Azimuth, deg	Inclination, deg	Magnitude, bars
σ_1	122	0	100
σ_2	32	0	30
σ_3	122	90	0

[a]The principal compression axis for this stress tensor, along with optimal orientations of thrust and strike-slip faults far from the Chi-Chi source, are shown in Figures 7b and 7c.

sites of very low background seismicity rate do not light up in aftershocks regardless of the Coulomb stress increase or their proximity to the main shock rupture surface.

4.2. Seismicity Rate Decreases in the Stress Shadows

[32] We observe a widespread seismicity rate jump within 150 km of the Chi-Chi epicenter during the first several months of the main shock. Following this initial period, there are four principal regions of sustained seismicity rate declines. These seismicity rate drops are evident in uniform cell sampling (Figures 4b and 4c), and can be visually confirmed by $M \geq 2$ seismicity where background rates are low (Figures 1a and 1b), and by in all cases by $M \geq 3$ seismicity (Figure 5). In these regions the seismicity rate changes are statistically significant, and drop by 40–90% (Figure 6 and Table 1). The Nansan and Kaoping zones, which enlarge over the 50 months after Chi-Chi, fall into the Coulomb stress shadows for strike-slip faults but not for thrust faults. Focal mechanisms of pre- and post-Chi-Chi earthquakes in these zones are dominated by strike-slip events (Figure 9b). For Huatung, which has the highest background seismicity rate, the seismicity rate may recover to pre-Chi-Chi levels by the end of the 50-month period, behavior would be consistent with rate/state friction if the stressing rate were higher there than elsewhere.

[33] The sites of seismicity rate changes resemble the calculated Coulomb stress change, whether we use a simple, idealized source (Figures 7b and 7c) or the detailed source (Figures 9a–9c), from which we conclude that the stress shadows do, indeed, cause the rate of earthquakes to drop. The existence of four zones of post-Chi-Chi seismicity rate drop, and their association with Coulomb stress shadows, is a critical validation of the Coulomb hypothesis, because it is an attribute unique to the static stress change. Observations of seismicity rate drops are only possible when background seismicity rates are high and seismic station is dense. *Felzer and Brodsky* [2005] argue that seismicity rate declines associated with main shocks do not occur, and take issue with reported rate declines associated with the 1989 $M = 6.9$ Loma Prieta [*Parsons*, 2002], 1983 $M = 6.7$ Coalinga [*Toda and Stein*, 2002], and 1992 Landers [*Wyss and Wiemer*, 2000] shocks. In our judgment, the Chi-Chi result, together with similar findings for the 1997 $M = 6.5$ Kagoshima [*Toda and Stein*, 2003; *Woessner et al.*, 2004] and 1999 $M = 7.1$ Hector Mine [*Toda et al.*, 2005] shocks, strengthens the case for the role of stress shadows in suppressing seismicity.

4.3. Focal Mechanisms Confirm the Role of Coulomb Stress Changes

[34] When we shed the optimal orientation assumption and resolve stress changes on the nodal planes of the post-Chi-Chi shocks: 85% of the thrust and 65% of the strike-slip events receive calculated shear stress increases greater than 0.1 bar; this compares with 37% of the thrust and 49% of the strike-slip shocks during the pre-Chi-Chi period, for which no correlation would be expected. To examine the Coulomb stress, which includes the role of unclamping in promoting failure, we measure the percentage increase after the Chi-Chi earthquake. Here we find a 26% increase in thrust events, and an 18% increase in strike-slip events receiving a Coulomb stress change greater than 0.1 bar. By comparison, *Hardebeck et al.* [1998] reported a 25% increase for Landers, *Hardebeck and Hauksson* [1999] reported a 20% increase for Northridge, and *Seeber and Armbruster* [2000] found a 30% increase for Landers (all three results are replotted in Figure 5 of *Stein* [1999]). Finally, no other main shock examined by Coulomb analysis has Chi-Chi's abundance of large aftershocks; 7–9 out of 10 $M \geq 6$ shocks receive a positive Coulomb stress change, with a mean stress increase of 4.4 bars.

4.4. Is the Signature of Dynamic Stress Triggering Visible in the First Postseismic Months?

[35] The widespread seismicity rate increase lasting for 1–3 months after Chi-Chi (Figures 4a and 6) could be caused by dynamic stress triggering. *Parsons* [2002] ob-

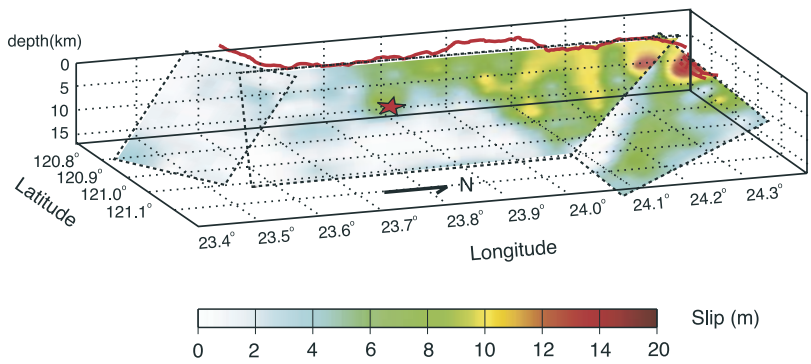

Figure 8. Slip distribution from *Ji et al.* [2003], with a main segment 80-km-long north-south segment, a 20-km-long segment to the southwest and a 30-km-long segment to the northeast. Each fault segment has a width of about 34 km and dips 29° to the east. The fault plane in each segment was approximated by the subfaults with equal area of 3.8 km × 3.7 km.

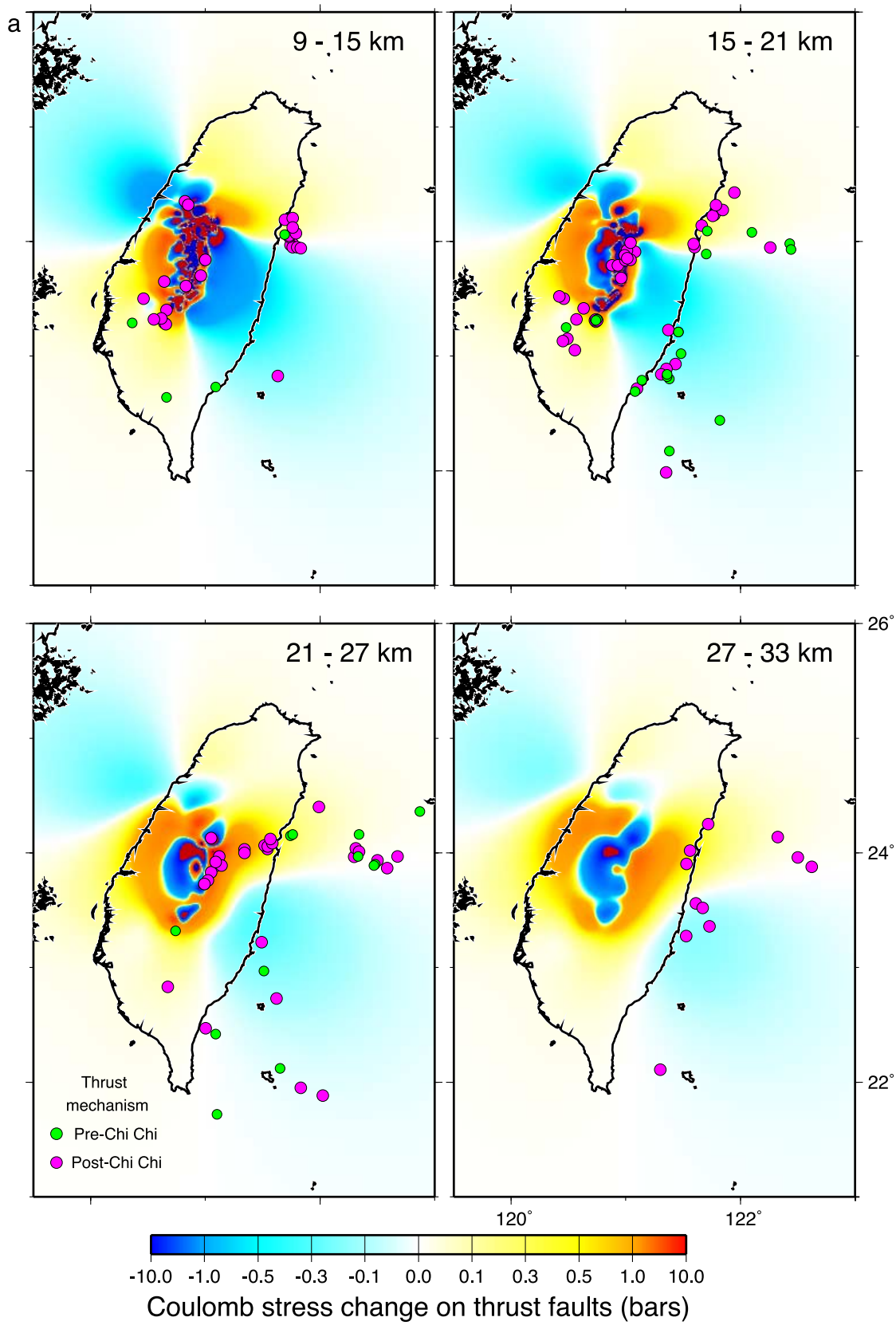

Figure 9. Coulomb stress changes on optimally oriented (a) thrust, (b) strike-slip, and (c) normal faults at four depth intervals, together will all $M \geq 4$ shocks with focal mechanisms. Stress is calculated at the center of each interval. Green shocks occurred during the 50 months before Chi-Chi, magenta shocks struck during the succeeding 50 months. Shallower intervals are not shown because no focal mechanisms are located above 9 km depth.

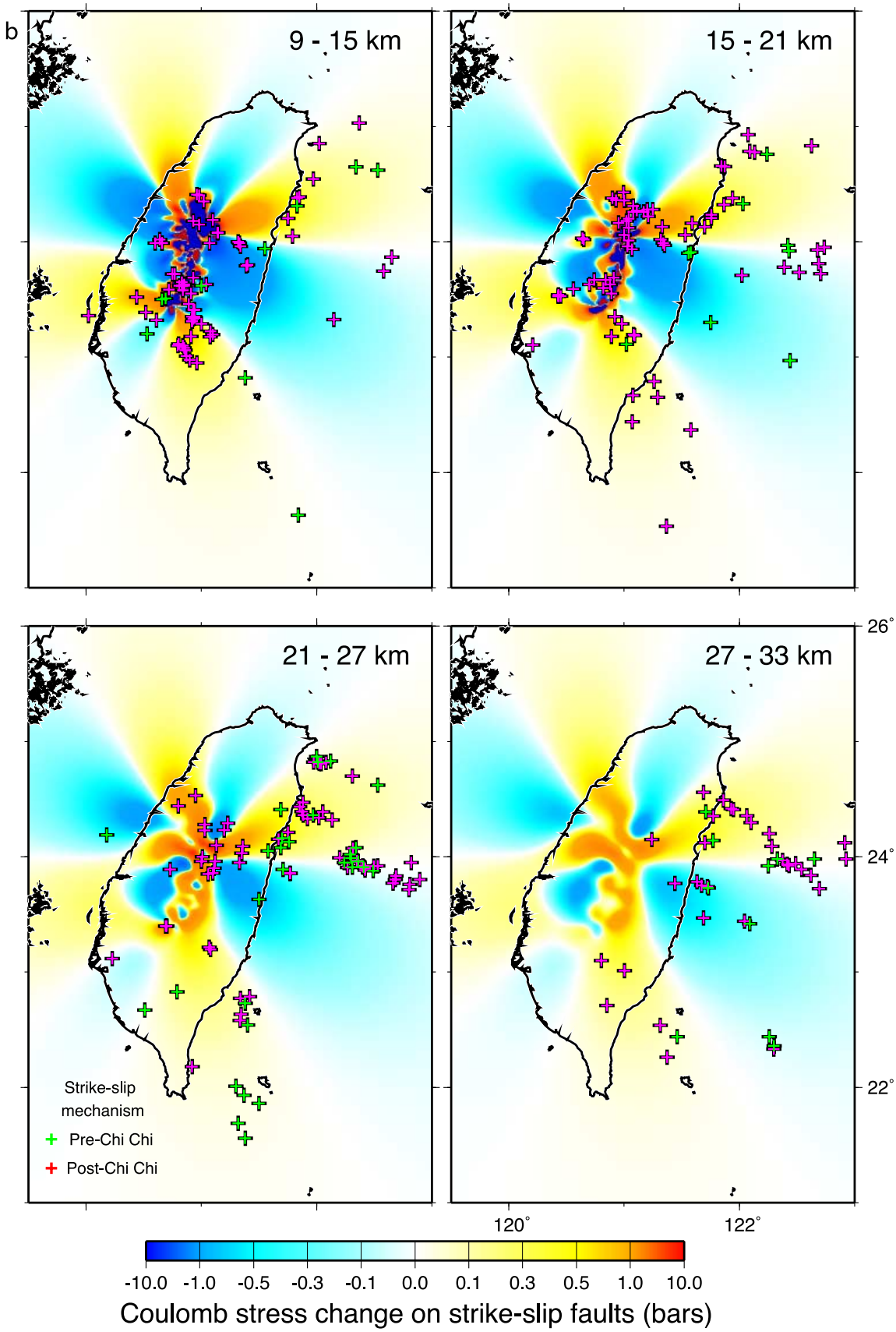

Figure 9. (continued)

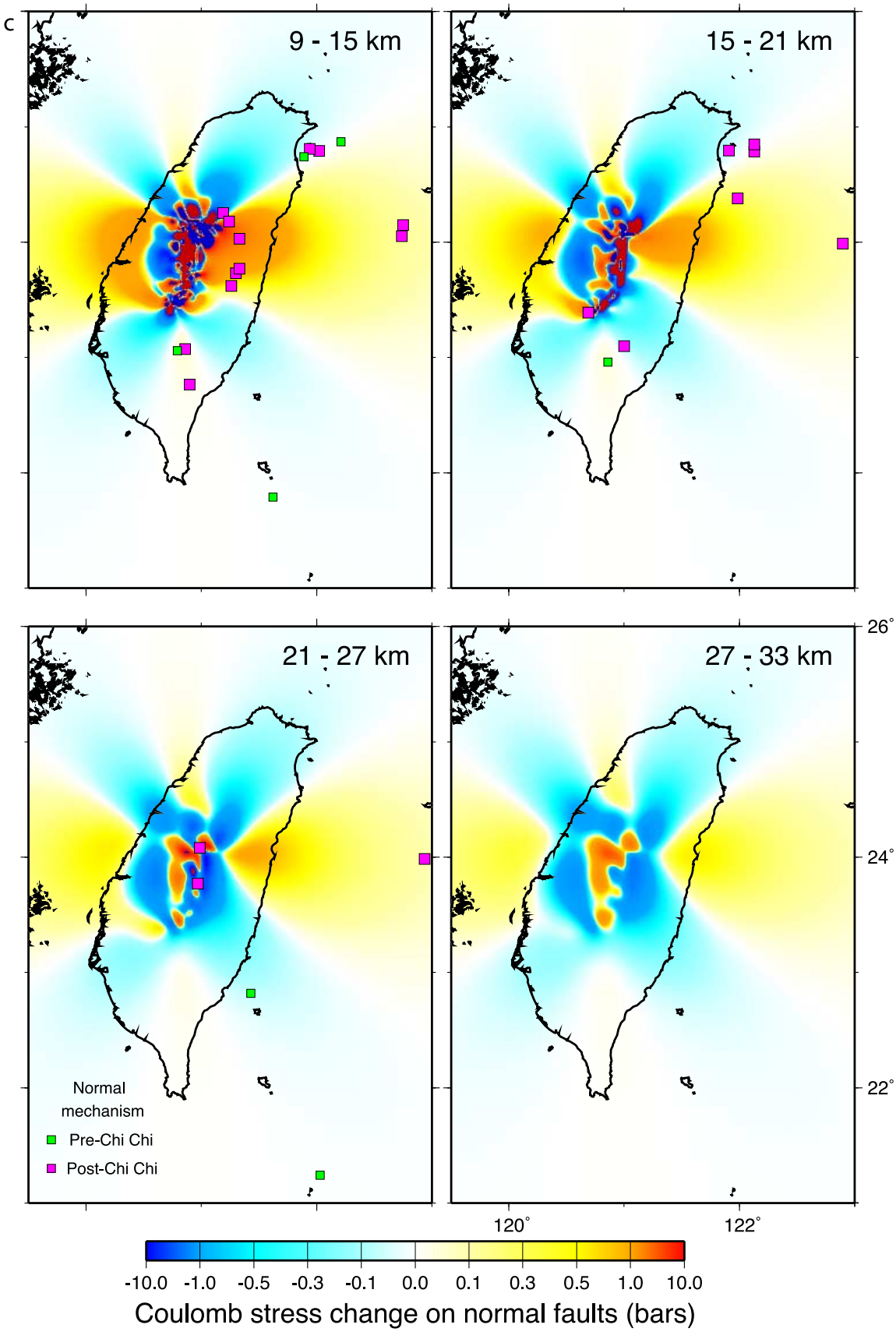

Figure 9. (continued)

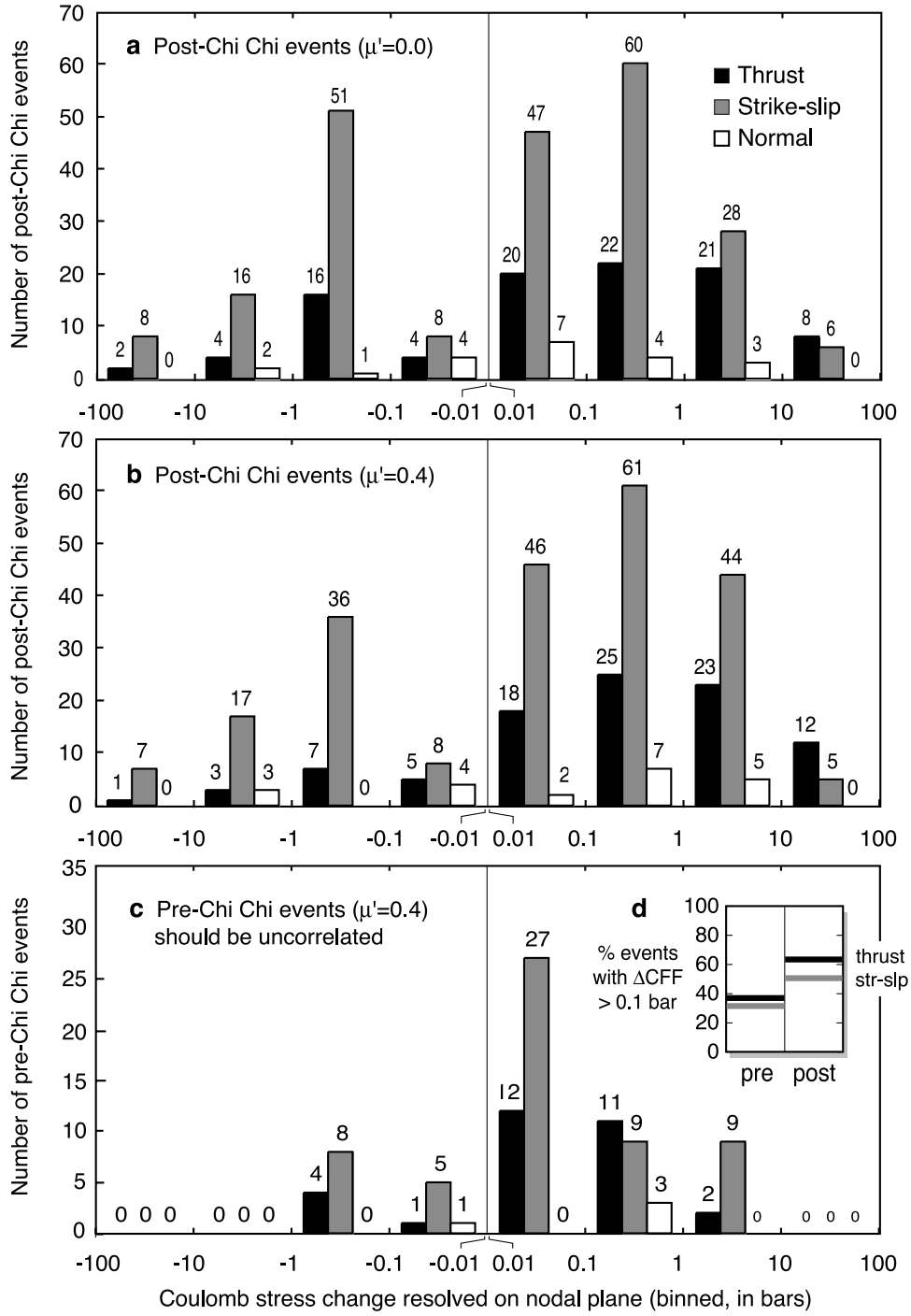

Figure 10. Stress change on nodal planes for all events with focal mechanisms. (a) Shear stress change on post-Chi-Chi nodal planes. (b) Coulomb stress change. For earthquakes with positive ΔCFF values on either nodal plane, the smaller of the two is chosen. For the earthquakes for which only one nodal plane has a positive ΔCFF, the positive one is chosen. For the events with negative ΔCFF on both nodal planes, the smaller absolute value is chosen. (c) Coulomb stress change calculated in the same manner for the pre-Chi-Chi focal mechanisms, which serves as a control sample. (d) Percentage of nodal planes with a calculated Coulomb stress change greater than 0.1 bar for the pre- and post-Chi-Chi periods, showing an increase following the Chi-Chi main shock.

served a similar phenomenon following $M \geq 7$ shocks in the Harvard CMT catalog, in which regions within 100 km of the main shock subjected to a calculated shear stress drop showed a fivefold increase in seismicity rate during the first binned interval, in this case, 1 yr. A similar but somewhat muted rate increase on planes calculated to be subjected to a Coulomb stress decrease following the 1992 Landers earthquake is apparent for the initial 2–4 months in time the

Table 3. Coulomb Stress Changes (for $\mu' = 0.4$) Imparted by the Chi-Chi Main Shock, and by Chi-Chi Plus Successive $M \geq 6$ Shocks, Resolved Onto the Preferred Plane of Each $M \geq 6$ Shock That has Struck Since Ch-Chi[a]

Time, UT	Reference	Mag M_w	Depth, km	Longitude, deg	Latitude, deg	Strike, deg	Dip, deg	Rake, deg	Chi-Chi ΔCFF, bars	Cumulative ΔCFF, bars
1757:15	*Chi and Dreger* [2004]	6.4	8	121.01	23.94	200	41	78	−1.9	−1.9
1803:41	*Chi and Dreger* [2004]	6.2	8	120.86	23.81	0	10	80	57.9	57.9
	Yen [2002]	6.2	18	120.88	23.79	23	33	95	3.1	3.2
1811:53	*Yen* [2002]	6.1	24	121.06	23.85	209	85	139	7.3	−5.7
1816:16	*Yen* [2002]	6.1	21	121.04	23.84	336	38	63	14.8	14.6
2146:38	*Chi and Dreger* [2004]	6.6	18	120.82	23.60	330	89	15	2.6	2.5
	Yen [2002]	6.3	12	120.82	23.60	75	67	186	7.8	7.8
0014:41	*Chi and Dreger* [2004]	6.2	10	121.08	23.81	165	70	100	6.9	7.1
	Yen [2002]	6.2	29	121.05	23.83	314	26	43	3.0	2.9
2352:49	*Chi and Dreger* [2004]	6.8	16	121.01	23.87	5	30	100	11.5	11.3
	Yen [2002]	6.4	15	121.01	23.86	32	32	102	13.2	11.9
0218:56	*Chi and Dreger* [2004]	6.4	16	120.45	23.53	20	75	90	0.3	0.3
	Ma and Wu [2001]	6.4	17	120.43	23.52	180	42	56	0.0	0.0
0310:17	*Ma and Wu* [2001]	6.0	17	120.43	23.53	60	90	170	0.3	−1.7
1823:00	DMC-IES	6.1	27	121.11	23.9	296	24	−8	5.7	6.0
						33	87	−114	2.2	2.3
									4.4[b]	3.0[b]
									8.4[c]	7.4[c]

[a]Earthquakes are mapped in Figure 2b inset. No preferred plane has been proposed for event 10.
[b]Median.
[c]Average.

series of *Seeber and Armbruster* [2000]. Similarly, where the shear stress shadow of the 1983 Coalinga earthquake is traversed by the San Andreas fault, the seismicity rate does not drop for 4 months [*Toda and Stein*, 2002]. A region along the Landers rupture subjected to Coulomb stress drop by the 1999 $M = 7.1$ Hector Mine shock [*Toda et al.*, 2005, Figure 3b] shows a spike in seismicity lasting for the first 10 days. However, in contrast, the seismicity rate decrease associated with the second of the 1997 Kagoshima couplet either is immediate [*Toda and Stein*, 2003, Figure 8a] or perhaps begins within 5 days [*Woessner et al.*, 2004, Figure 3].

[36] Ascribing the initial seismicity rate distribution to the dynamic stresses is made difficult at Chi-Chi because there is little evident rupture directivity [*Aagard et al.*, 2004], and so static and dynamic patters may be unusually similar. Further, while the dynamic stresses would not exhibit seismicity rate drops [*Gomberg et al.*, 1998], the first 3 months represent too short a period to detect rate declines, and so their absence in the first 3 months need not indicate dynamic stressing. As suggested by *Parsons* [2005], it may be possible for dynamic stresses to excite an Omori lake aftershock sequence, which perhaps could have a more rapid decay constant than that triggered by the static stress changes. We suggest that a fruitful avenue of research would be to investigate this transient seismicity rate increase, to see where it might lead us in the quest to understand earthquake triggering.

[37] **Acknowledgments.** We are grateful for reviews by William Bakun, Delphine Fitzenz, Joan Gomberg, Ruth Harris, and two anonymous referees. We thank Yuh-Ing Chen for insight on M_c and W.-Z. Liang and the Central Weather Bureau Seismological Center for providing the complete seismic catalog and the BATS CMT solutions from DMC-IES. This work is partly funded by the Taiwan Ministry of Education, iSTEP 91-N-FA07-7-4. R.S. is grateful for support from Swiss Re.

References

Aagard, B. T., J. F. Hall, and T. H. Heaton (2004), Effects of fault dip and slip rake angles on near-surface ground motions: Why rupture directivity was minimal in the 1999 Chi-Chi, Taiwan, earthquake, *Bull. Seismol. Soc. Am.*, *94*, 155–170.

Chen, W.-S., K.-J. Lee, L.-S. Lee, D. J. Ponti, C. Prentice, Y.-G. Chen, H.-C. Chang, and Y.-H. Lee (2004), Paleoseismology of the Chelungpu fault during the past 1900 years., *Quat. Int.*, *115–116*, 167–170.

Chi, W.-C., and D. Dreger (2004), Crustal deformation in Taiwan: Results from finite source inversions of six $M_w > 5.8$ Chi-Chi aftershocks, *J. Geophys. Res.*, *109*, B07305, doi:10.1029/2003JB002606.

Chi, W.-C., D. Dreger, and A. Kaverina (2001), Finite-source modeling of the 1999 Taiwan (Chi-Chi) earthquake derived from a dense strong-motion network, *Bull. Seismol. Soc. Am.*, *91*, 1144–1157.

Dieterich, J. (1994), A constitutive law for rate of earthquake production and its application to earthquake clustering, *J. Geophys. Res.*, *99*(B2), 2601–2618.

Felzer, K. R., and E. E. Brodsky (2005), Testing the stress shadow hypothesis, *J. Geophys. Res.*, *110*, B05S09, doi:10.1029/2004JB003277.

Gomberg, J., N. M. Beeler, M. L. Blanpied, and P. Bodin (1998), Earthquake triggering by transient and static deformations, *J. Geophys. Res.*, *103*, 24,411–24,426.

Hardebeck, J. L., and E. Hauksson (1999), Background stress state plays a role in earthquake triggering, *Eos Trans. AGU*, *80*(46), Fall Meet. Suppl., 1005.

Hardebeck, J. L., J. J. Nazareth, and E. Hauksson (1998), The static stress change triggering model: Constraints from two southern California aftershocks sequences, *J. Geophys. Res.*, *103*, 24,427–24,437.

Harris, R. A. (1998), Introduction to special section: Stress triggers, stress shadows, and implication for seismic hazard, *J. Geophys. Res.*, *103*, 24,347–24,358.

Ji, C., D. V. Helmerger, D. J. Wald, and K.-F. Ma (2003), Slip history and dynamic implications of the 1999 Chi-Chi, Taiwan, earthquake, *J. Geophys. Res.*, *108*(B9), 2412, doi:10.1029/2002JB001764.

Kao, H., Y.-H. Liu, W.-T. Liang, and W.-P. Chen (2002), Source parameters of regional earthquakes in Taiwan: 1999–2000 including the Chi-Chi earthquake sequence, *Terr. Atmos. Oceanic Sci.*, *13*, 279–298.

King, G. C. P., and M. Cocco (2001), Fault interaction by elastic stress changes: New clues from earthquake sequences, *Adv. Geophys.*, *44*, 1–28.

King, G. C. P., R. S. Stein, and J. Lin (1994), Static stress changes and the triggering of earthquakes, *Bull. Seismol. Soc. Am.*, *84*, 935–953.

Liang, W.-T., Y.-H. Liu, and H. Kao (2003), Source parameters of regional earthquakes in Taiwan: January–December 2001, *Terr. Atmos. Oceanic Sci.*, *14*, 249–260.

Liang, W.-T., Y.-H. Liu, and H. Kao (2004a), Source parameters of regional earthquakes in Taiwan: January–December 2002, *Terr. Atmos. Oceanic Sci.*, *15*, 727–741.

Liang, W. T., Y. H. Liu, H. Kao, and B. S. Huang (2004b), Introduction to the centroid moment tensor catalog database of Taiwan: A key issue of the broadband array in Taiwan for seismology (BATS), paper presented at XXIX Gen. Assembly, Eur. Seismol. Comm., Potsdam, Germany.

Lin, J., and R. S. Stein (2004), Stress triggering in thrust and subduction earthquakes, and stress interaction between the southern San Andreas and nearby thrust and strike-slip faults, *J. Geophys. Res.*, *109*, B02303, doi:10.1029/2003JB002607.

Ma, K.-F., and L.-Y. Chiao (2003), Rupture behavior of the 1999 Chi-Chi, Taiwan, earthquake-slips on a curved fault in response to the regional plate convergence, *Eng. Geol.*, *71*, 1–11.

Ma, K.-F., and S.-I. Wu (2001), Quick slip distribution determination of moderate to large inland earthquakes using near-source strong motion waveforms, *Earthquake Eng. Earthquake Seismol.*, *3*, 1–10.

Ma, K.-F., J. Mori, S.-J. Lee, and S.-B. Yu (2001), Spatial and temporal distribution of slip for the 1999 Chi-Chi, Taiwan earthquake, *Bull. Seismol. Soc. Am.*, *91*, 1–19.

Marsan, D. (2003), Triggering of seismicity at short timescales following Californian earthquakes, *J. Geophys. Res.*, *108*(B5), 2266, doi:10.1029/2002JB001946.

Parsons, T. (2002), Global Omori law decay of triggered earthquakes: Large aftershocks outside the classical aftershock zone, *J. Geophys. Res.*, *107*(B9), 2199, doi:10.1029/2001JB000646.

Parsons, T. (2005), A hypothesis for delayed dynamic earthquake triggering, *Geophys. Res. Lett.*, *32*, L04302, doi:10.1029/2004GL021811.

Parsons, T., R. S. Stein, R. W. Simpson, and P. A. Reasenberg (1999), Stress sensitivity of fault seismicity: A comparison between limited-offset oblique and major strike-slip faults, *J. Geophys. Res.*, *104*, 20,183–20,202.

Press, W. H., S. A. Teukolsky, W. T. Vetterling, and B. P. Flannery (1992), *Numerical Recipies in Fortran: The Art of Scientific Computing*, 964 pp., Cambridge Univ. Press, New York.

Seeber, L., and J. G. Armbruster (2000), Earthquakes as beacons of stress change, *Nature*, *407*, 69–72.

Seno, T. (1977), The instantaneous rotation vector of the Philippine Sea Plate relative to the Eurasian Plate, *Tectonophysics*, *42*, 209–226.

Stein, R. S. (1999), The role of stress transfer in earthquake occurrence, *Nature*, *402*, 605–609.

Stein, R. S., G. C. P. King, and J. Lin (1994), Stress triggering of the 1994 $M = 6.7$ Northridge, California, earthquake by its predecessors, *Science*, *265*, 1432–1435.

Toda, S., and R. S. Stein (2002), Response of the San Andreas fault to the 1983 Coalinga-Nuñez earthquakes: An application of interaction-based probabilities for Parkfield, *J. Geophys. Res.*, *107*(B6), 2126, doi:10.1029/2001JB000172.

Toda, S., and R. S. Stein (2003), Toggling of seismicity by the 1997 Kagoshima earthquake couplet: A demonstration of time-dependent stress transfer, *J. Geophys. Res.*, *108*(B12), 2567, doi:10.1029/2003JB002527.

Toda, S., R. S. Stein, P. A. Reasenberg, J. H. Dieterich, and A. Yoshida (1998), Stress transferred by the $M_w = 6.9$ Kobe, Japan, shock: Effect on aftershocks and future earthquake probabilities, *J. Geophys. Res.*, *103*, 24,543–24,565.

Toda, S., R. S. Stein, K. Richards-Dinger, and S. Bozkurt (2005), Forecasting the evolution of seismicity in southern California: Animations built on earthquake stress transfer, *J. Geophys. Res.*, *110*, B05S16, doi:10.1029/2004JB003415.

Waldhauser, F., and W. L. Ellsworth (2000), A double-difference earthquake location Algorithm: Method and application to the northern Hayward fault, California, *Bull. Seism. Soc. Am.*, *90*, 1353–1368.

Wang, J.-C., C.-F. Shieh, and T.-M. Chang (2003), Static stress changes as a triggering mechanism of a shallow earthquake: Case study of the 1999 Chi-Chi (Taiwan) earthquake, *Phys. Earth Planet. Inter.*, *135*, 17–25.

Wang, W.-H., and C.-H. Chen (2001), Static stress transfer by the 1999 Chi-Chi, Taiwan, earthquake: Effects on the stability of the surrounding fault systems and aftershock triggering with a 3D fault-slip model, *Bull. Seismol. Soc. Am.*, *91*, 1041–1052.

Wang, W.-H., S.-H. Chang, and C.-H. Chen (2001), Fault slip inverted from surface displacements during the 1999 Chi-Chi, Taiwan, earthquake, *Bull. Seismol. Soc. Am.*, *91*, 1167–1181.

Wiemer, S. (2001), A software package to analyse seismicity: ZMAP, *Seismol. Res. Lett.*, *72*(3), 373–382.

Wiemer, S., and M. Wyss (2000), Minimum magnitude of completeness in earthquake catalogs: Examples form Alaska, the western United States, and Japan, *Bull. Seismol. Soc. Am.*, *90*, 859–869.

Woessner, J., E. Hauksson, S. Wiemer, and S. Neukomm (2004), The 1997 Kagoshima (Japan) earthquake doublet: A quantitative analysis of aftershock rate changes, *Geophys. Res. Lett.*, *31*, L03605, doi:10.1029/2003GL018858.

Wyss, M., and S. Wiemer (2000), Change in probability for earthquakes Landers in southern California due to the magnitude 7.3 earthquake, *Science*, *290*, 1334–1338.

Yen, Y.-T. (2002), Slip distribution of $M_w > 6.0$ aftershocks of the 1999 Chi-Chi Taiwan earthquake, M.Sc. Dissertation, 122 pp., Natl. Cent. Univ., Taiwan.

Zeng, Y. H., and C. H. Chen (2001), Fault rupture process of the 20 September 1999 Chi-Chi, Taiwan, earthquake, *Bull. Seismol. Soc. Am.*, *91*, 1088–1098.

C.-H. Chan and K.-F. Ma, Institute of Geophysics, National Central University, 100 Chung-Da Road, Chung-Li 320-54, Taiwan. (fong@earth.ncu.edu.tw)

R. S. Stein, U.S. Geological Survey, 345 Middlefield Road, MS 977, Menlo Park, CA 94025, USA. (rstein@usgs.gov)